PAPER • OPEN ACCESS

Photolithographic nanoseeding method for selective synthesis of metal-catalysed nanostructures

View the article online for updates and enhancements.

Photolithographic nanoseeding method for selective synthesis of metal-catalysed nanostructures

J Marques-Hueso[1,5] , J A S Morton[1], Xiangfu Wang[2,5] ,
E Bertran-Serra[3,4] and M P Y Desmulliez[1]

[1] Microsystems Engineering Centre, Institute of Sensors, Signals and Systems, Heriot-Watt University, Edinburgh, United Kingdom
[2] College of Electronic and Optical Engineering & College of Microelectronics, Nanjing University of Posts and Telecommunications, Nanjing, People's Republic of China
[3] FEMAN Group, Departament de Física Aplicada, Universitat de Barcelona, Barcelona, Spain
[4] Institute of Nanoscience and Nanotechnology, IN2UB, Universitat de Barcelona, Barcelona, Spain

E-mail: j.marques@hw.ac.uk and xfwang@njupt.edu.cn

CrossMark

Abstract

In this work we present a general method for the selective synthesis by photolithography of localised nanostructures in planar geometries. The methodology relies on the previous concept of photo-patternable metallic nanoparticle (NP)/polymer nanocomposites, which can provide a range of NP sizes, polydispersity and densities. First, a photoresist containing metallic ions is patterned by photolithography. Silver NPs are synthesised *in situ* after the exposure and development of the patterned thin film via the thermal-induced reduction of ions embedded in its structure. Gentle plasma ashing is used to selectively remove the polymer, which leaves NPs on the patterned areas. These NPs are used as seeds for subsequent processes. In order to demonstrate the flexibility of the method, its use to selectively produce localised nanostructures through different processes is shown here. Following a top-down approach, high aspect-ratio silicon nanograss has been produced by reactive ion etching and masking by the NPs. In a bottom-up approach, 280 nm copper clusters have been selectively grown in arrays. This method can be easily extrapolated to other metals and it provides a quick way to selectively generate hierarchical nanostructures in large planar areas that can be used for different applications, such as the fabrication of nanostructured sensor arrays.

Keywords: silver nanoparticle, nanoseeding, nanocomposite, photopatterning, silicon nanotips, selective synthesis

(Some figures may appear in colour only in the online journal)

1. Introduction

Unconventional nanofabrication techniques [1] have attracted much attention due to their potential use in a large number of applications that can benefit from low-dimensional materials. For example, a remarkable application of such a technique is the deposition or fabrication of metallic nanostructures on a flat substrate, especially noble metals, using photopatterning. Metallic nanoparticles (NPs) are useful for optical techniques like surface-enhanced Raman scattering [2], sensing [3], and

[5] Authors to whom any correspondence should be addressed.

1

surface-enhanced fluorescence [4]. Moreover, they are one of the most commonly used catalysers for the growth of other nanostructures. Often, the development of new nanostructures starts indeed with the patterning of the substrate followed by a top-down or bottom-up approach, or a combination of both.

Most of the common nanofabrication techniques provide high resolution or high throughput, where the most challenging case is when small nanostructures are desired to be selectively placed along extended areas at a low cost [5]. Electron beam lithography, focused ion beam milling and pulsed laser [6] offer very high resolution for both the shape and position of the NP, at the expense however of low throughput. Other approaches have been proposed to produce extended ordered nanostructure arrays, such as the use of block copolymer templates [7], laser interference synthesis [8], directed self-assembly [9] or colloidal lithography [10, 11]. At the same time, other techniques offer very high throughputs for random distributed NPs, such as thin film annealing [12]. For the latter, the control on two parameters, the deposited metal thickness and the temperature bake, gives rise to a limited range of sizes and densities of NPs.

The use of polymer as a host for the *in situ* synthesis of NPs offers clear advantages in terms of control over size, shape, density and size dispersity of the NPs [13]. This synthesis consists of using polymers that have functional groups with the redox capability to reduce embedded metallic ions to the corresponding NPs [14]. In this way, the introduction of polymer facilitates the control on size and dispersity, which are important if the NPs are going to be used as precursors. Moreover, the presence of the polymer allows the NPs to be synthesised at a relatively low temperature (even less than 150 °C), while other techniques like the formation of Ag droplets by annealing very then films (approx. 1 nm) can reach temperatures of 650 °C [15, 16].

Some lithographic polymeric compounds present this reducing ability, which enables the synthesis of NPs in a small volume of polymer that has been defined by a lithographic technique [17]. Poly-vinyl-alcohol has been shown to be a suitable host for synergetic electron beam lithography, and gold [18] and silver [19] NP synthesis. This technique allows the placement of NPs in the range of 10 nm in size with a spatial resolution of 180 nm [18]. More importantly, UV-patternable novolac phenol-formaldehyde resins sensitised with diazo-naphthoquinone (DNQ) have also shown this reducing capability, both in their positive [20] and negative [21] formulation, and for gold and silver NPs [21]. By using this host, it is possible to synthesise NPs ensembles in areas patterned by UV-lithography with the corresponding resolution. Moreover, by controlling the post-bake parameters and initial metal molarity, it is possible to have some control over the size and distribution of the NPs, and it is not difficult to produce monodispersed NPs smaller than 10 nm [20, 22]. This point is important because some nanostructures, such as semiconductor nanowires, benefit from reduced diameters [23].

UV-lithography offers many advantages. For a resolution just below one micron, the equipment can be reduced to a simple mercury bulb to provide 436 nm (g-line) or 365 nm (i-line) light. Excimer lasers (248 nm from KrF and 193 nm from ArF) have enabled the patterning of features down to 32 nm. Smaller features are possible by deep ultraviolet lithography together with the immersion and double patterning techniques. The next technology, extreme ultraviolet lithography, is able to provide 13 nm line/space half-pitch resolution [24], albeit at a high cost.

Once the metallic NPs have been synthesised in the desired areas, they can be used to generate other structures. Ag and Au NPs can catalyse carbon nanotube growth by CVD [25]. NPs also constitute the seeds for the growth via vapour–liquid–solid (VLS) technique [26]. Although gold is the most used catalyser, other metals [27] such as silver and copper can also trigger the vertical or horizontal [28] growth of nanowires of relevant materials such as silicon [29], oxides [30] and compound semiconductors [31]. In addition, Ag NPs have shown to be reliable seeds in order to create conductive tracks by electroless plating [32].

Metallic NPs can also be used to generate silicon nanograss, also known as nanotips, nanocones, or black silicon, depending on the size, aspect-ratio and application. Its applications range from antimicrobial surfaces [33] and modification of optical properties [34] to improved electrochemical anodes for batteries [35]. There are different ways to fabricate black silicon [36, 37] such as metal-assisted wet chemical etching [38], electrochemical etch, laser ablation or reactive ion etching (RIE). Many of these methods have been patented. Additionally, hierarchical arrays can be produced by the combination of two of these techniques [34]. In the case of RIE, the commonly used chemistry [37] is $SF_6 + O_2$, where the fluorine radicals generated from the SF_6 provide the silicon etch, and the O_2 allows the production of SiO_xF_y for wall passivation. Other well-known chemistry [39] is $SF_6 + O_2 + CHF_3$, where small amounts of CHF_3 are the source for the CF radicals which etch the SiO_xF_y layer in one direction forming the volatile CO_xF_y. Hence, the addition of further CHF_3 avoids the nanograss formation [39], and a composition of $SF_6 + CHF_3$ is a well-known chemistry for silicon anisotropic etch. $SF_6 + O_2 + CHF_3$ is also a very good polymer etcher, and etch rates as high as 5000 nm min^{-1} have been reported [39]. This prevents the use of photoresist masking for selective fabrication of small silicon structures. On the other hand, the metals and metal-oxides are not affected by this etch and provide a virtually infinite selectivity with respect to silicon [39, 40].

In this work, we have developed a new method based on the use of Ag/DNQ-novolac lithographic nanocomposites in order to generate nanoseeds for further nano-synthesis processes. The method allows the patterning of extended areas by photolithography using an inexpensive UV-lamp and a chrome mask. Next, small NPs are synthesised in the remainder resist by a thermally driven chemical reduction of embedded silver ions. An optimised plasma treatment removes the polymer that covers the NPs, so that they are more accessible for further nano-synthesis processes. Then, as

a proof-of-concept, we have applied the seeding method for the creation of black silicon in selected areas by using the NPs as hard mask for RIE. Finally, we have used the method for the selective synthesis of copper clusters of 280 ± 150 nm by electroless plating.

This method is an easy and quick tool that could find further application in other fields of nanotechnology, such as selective catalysed synthesis of nanostructures, VSL growth, or seeded plating.

2. Methods

2.1. Fabrication

0.015 g AgClO4 is diluted in 0.5 ml 1-methoxy 2-propylacetate (MPA). After complete dissolution, the solution is added to 2 ml of S1805 novolac-based photoresist (MICROPOSIT™ S1805 positive photoresist, Dow (R)—Shipley/Rohm & Haas). The solution (from now 'modified photoresist') is spin-coated at 4000 rpm on silicon and glass substrates, which are then left on a hot-plate at 45 °C during 2 min. The films are exposed in an ultraviolet crosslinker (CL-1000 UVP, equipped with five Hitachi F8T5 bulbs) at 100 mJ cm^{-2}, using a chromium mask to define patterns. The samples are then developed during 5 s in a solution of tetramethylammonium hydroxide (TMAH) in water (1:10 volume). Immediately, they are immersed in water during 5 s and dried with compressed nitrogen. The samples are then baked at 210 °C during 15 s on a hot-plate, which produces the silver NPs. This process results in 342 ± 11 nm thick films.

The oxygen plasma treatment is run out in a RIE chamber Plasmalab μPRIE80. The RF power is set at 200 W, the O_2 flow at 10 sccm, and the time varies from 30 to 120 s. The resulting pressure is 30 mTorr and the generated DC bias is 340 V.

The silicon dry etch has been carried out in an Oxford Instruments Plasmalab 65 ICP system. The gas mixture is composed of SF_6 (5 sccm) and CHF_3 (70 sccm) at a pressure of 8 mTorr, and the plasma has been produced with 20 W of RF in the main chamber and 200 W in the ICP column, during 6 min.

The copper cluster synthesis has been obtained by immersion in a solution comprising of 15 g L^{-1} copper (II) sulphate pentahydrate, 20 g L^{-1} sodium hydroxide, 70 g L^{-1} sodium potassium tartrate and 77 ml L^{-1} formaldehyde 37%, at room temperature.

2.2. Characterisation

The optical absorption spectra of the films on glass were measured with a spectrophotometer (Perkin-Elmer, Lambda 950 UV/VIS/NIR) with a resolution of 1 nm over the 325–600 nm wavelength range. A clean glass substrate was used as reference for spectrophotometer calibration. The absorbance of the films is calculated from the difference between the transmission through the reference and through the sample, while the reflectance is neglected. The thicknesses of the films were measured using a Dektak3 surface profiler.
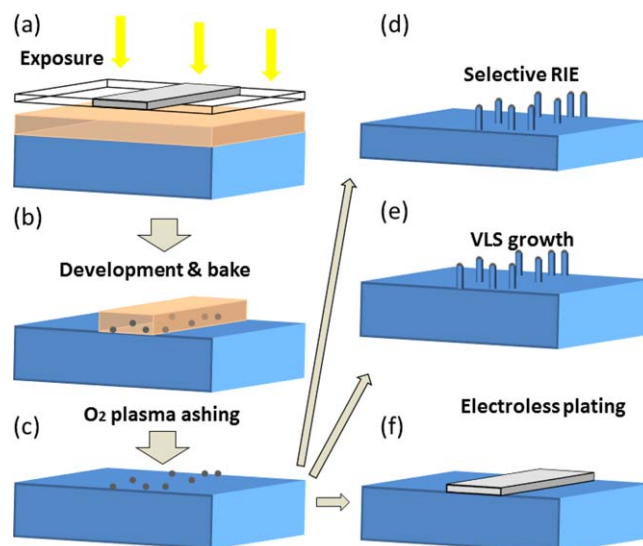

Figure 1. Flowchart of the nanoseeding method. (a) UV-lithography is performed to pattern the polymer, (b) the Ag NPs are synthesised during a short bake, (c) the polymer is selectively removed by using oxygen plasma and it leaves areas of NPs. After this, the selectively located NPs could be used for different purposes: as a hard mask for selective RIE (d), as catalyst for synthesis of nanostructures (e), or as seeding layer for electroless plating (f).

The SEM used for characterisation is a FEI Quanta 3D FEG. The silicon tips have been scraped by using a glass knife and deposited on a TEM carbon-copper grid previously wetted in D. I. water. A JEOL ARM200F scanning electron microscope has been used for the inspection.

The electron beam lithography has been carried out using a Raith Pioneer system at 30 KV. The exposure dose has been 80 μA cm^{-2}, by using steps of 14 nm with beam current of 0.26 nA. The development was performed as usual.

3. Results and discussion

3.1. Nanoseeding method

The process to create the patterns and the seeding method can be seen in the flowchart in figures 1(a)–(c). The UV-lithography has been performed by using the modified photoresist as explained at the experimental section. The polymer patterns are defined after the development, and a bake then produces the synthesis of NPs by reducing the Ag(III) ions with help of the polymer via thermal excitation. The size of the resulting Ag NPs in the DNQ/Novolac system is known to be controllable by tuning the temperature, as well as the NP density by controlling the initial metallic ion concentration [20]. Gentle oxygen plasma ashing is then used to remove the polymer and leave at least the larger silver NPs on the substrate (figure 1(c)). This constitutes the core of the nanoseeding method.

After this, different alternatives can be used to create nanostructures. In this work, and in order to show a complete proof-of-concept, selective RIE has been used to produce silicon nanograss by using the NPs as a hard mask for the
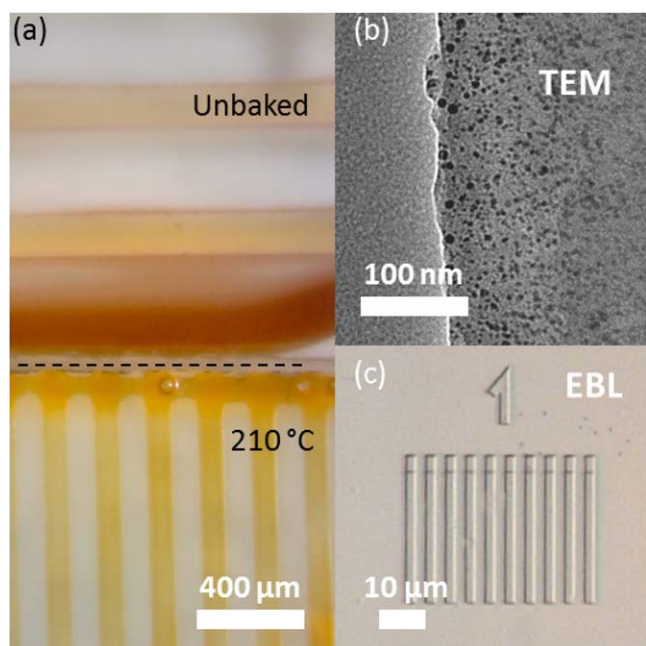
Figure 2. (a) Photograph of two glass samples with the UV-patterned nanocomposite, revealing the colour difference for baked and unbaked case (the dashed line marks the edges of both samples). (b) TEM of the nanocomposite, (c) image of the nanocomposite directly patterned by electron beam lithography and development (line width = 2 μm).

Figure 3. (a) Remaining thickness of the nanocomposite thin film after plasma treatment at different times, (b) SEM image of the sample treated 100 s, which clearly shows the boundary between areas with and without NPs.

etching (figure 1(d)). However, once the NPs remain on the surface of the substrate, they could be used as seeds for different techniques. For example, their metallic nature could be used to catalyse the vertical growth of nanowires by VLS method or molecular beam epitaxy (figure 1(e)). Alternatively, they could be used as a seeding layer to produce a metallisation by electroless plating (figure 1(f)).

Figure 2(a) shows the resulting UV-patterned nanocomposite of two samples, one before (top sample) and one after baking (bottom sample). Both samples have been included in the same photograph for accurate colour comparison. The image corresponds to the edge of the glass substrates, where the resist is always thicker after spin-coating due to the bead effect. The spin-coated films on glass show that the colour of the resist is modified during the baking process, as a result of the silver NP synthesis. Silver NPs present LSPR around 420 nm, which translates in a higher optical absorption at that wavelength. This results in the reddish colour of the original resist turning yellow. The presence of NPs is confirmed by TEM (figure 2(b)). It is possible to see that the size distribution is heterogeneous, with a high polydispersity. The larger NPs are approximately 50 nm in diameter. The total density of NPs is relatively high; although it has to be considered that they are expected to be distributed along the volume, in this case, of a 342 nm thick film. The main advantage of producing the NPs inside the polymer rather than directly on the surface is that the properties of the matrix determine the size and polydispersity of the NPs [14], as well as allowing synthesis at much lower temperatures.
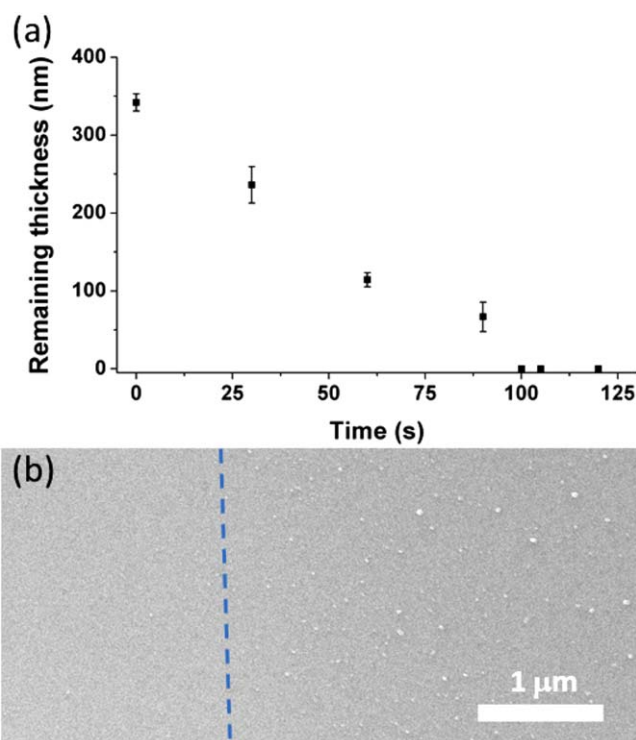
DNQ-novolac is a common photoresist used for UV patterning, but it also exhibits lithographic properties under electron beam exposure. In order to show the versatility of the material, a fresh solution has been spin-coated on silicon and allowed to dry at room temperature. Next, it has been patterned by electron beam lithography, and developed as usual. The results can be seen in the optical micrograph of figure 2(c), which shows the obtained pattern of 2 μm wide lines. EBL can achieve a very high resolution, although in our system the addition of metallic salts to the resist has a side-effect that can limit the resolution. The presence of the salts increases the solubility of the resist during the development, as can be deduced from the short processing times at the development stage.

Oxygen plasma is commonly used for the selective removal of polymers, and high removal ratios can be achieved. Similar novolac resists are usually removed at 300 nm min^{-1} [41] at 400 W and 300 mT. In this work, gentler ashing parameters have been used to remove the polymer while leaving the NPs as unaltered as possible. A large RIE chamber has been used in order to decrease the energy density of the plasma, and gas flow and pressure have been reduced as much as possible. Nanocomposite films on silicon dice have been treated at different ashing times, decreasing their thickness as shown in figure 3(a). An etching ratio of 196 nm min^{-1} has been achieved. Thanks to the good contrast on silicon, it is possible to see the patterns with the naked eye even for very thin films. The time to exhaust all the polymer has been determined to be 104 s. Silver is a heavy
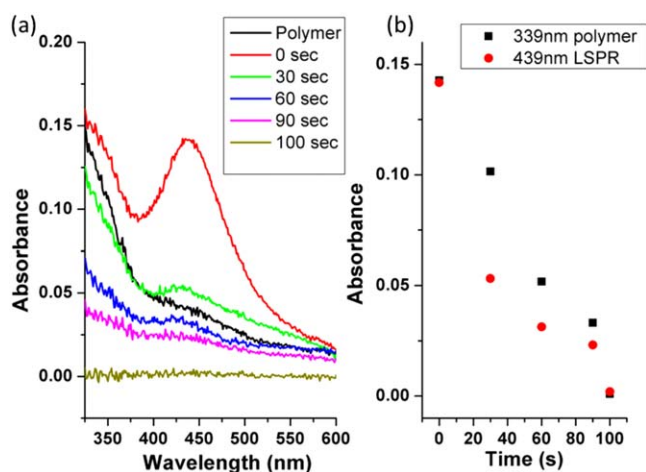
Figure 4. Optical absorbance of the nanocomposite films thinned at different times, (b) corresponding absorbance at the wavelengths 339 nm (due to polymer) and 439 nm (due to the NPs).

ion, which provides good contrast on silicon substrates at the SEM. Figure 3(b) shows the SEM of a sample ashed for 105 s. Although there is no more polymer, it is possible to see the patterns due to the remaining silver. A closer look reveals that the larger NPs are distinguishable, and the boundaries of patterned/unpatterned areas can be identified. The larger NPs are approximately 50 nm in diameter, which agrees with the TEM inspection in figure 2; the same applies to the relative spacing between them. The SEM of the patterned area shows a density of NPs lower than in the TEM image, although it has to be considered that smaller NPs can be present even if they are not visible under the SEM.

In order to obtain more information about the ashing process, the plasma treatment has been performed on nano-composite films on glass and their optical absorbance has been measured. Figure 4(a) shows the resulting spectra. The novolac resist presents significant absorption for wavelengths shorter than 380 nm as seen in the spectrum of a polymer reference without metallic ions (black line in figure 4(a)). At the same time, a nanocomposite film presents a high absorbance at 439 nm due to the SLPR of the silver NPs (red line in figure 4(a)). The asching process reduces the absorbance of the film in the entire spectrum, as expected. It is remarkable that the absorbance of the plasmon peak is greatly reduced during the first 30 s of plasma. For clarity, the absorbance at 339 nm (due to polymer) and at 439 nm (due to the NPs) for all the films has been represented in figure 4(b). The absorbance of the polymer at 339 nm decreases linearly with time, indicating thereby a linear etching rate. However, it is observed that the absorbance due to the silver NPs decreases faster than the peak due solely to the polymer in the first half of the process. The NPs are expected to be homogenously distributed in the volume. The thermal reduction of ions in polymer matrices tends to produce NPs distributed throughout the entire volume, while the chemical reduction can produce accumulation on the surface [42]. A possible explanation for the faster decrease of the absorbance at 439 nm could be the expected oxidation of the silver NPs in the plasma [43], which

could affect the plasmon resonance intensity. Moreover, the plasmon peak shifts from 439 to 431 nm during the first 30 s of plasma treatment. This could possibly be due to the reduction in size of the metallic core in the case of external oxidation, which would leave a smaller core and hence its plasmon resonance would be blue-shifted, as is happening. After 60 s, the reduction of the plasmon peak decreases in a slower manner, which could be due to the slower oxidation of the NPs.

Finally, another effect that can be observed in figure 3(a) is sudden decrease of the background absorbance from 90 to 100 s. This effect is due to the disappearance of the film as such in that interval. Even a very thin polymer film of a few nanometres causes reflection of the beam of the spectro-photometer. The reflectance for the case of normal incidence can be calculated from the Fresnel equations, and it follows the formula:

$$R = \left| \frac{n_1 - n_2}{n_1 + n_2} \right|^2$$

where n_2 is the refractive index of the medium (air), and n_1 of the material at the interface (polymer or glass). When the film disappears, the beam impinges the glass slide directly, which has a different refractive index than the polymer film and hence produces a different normal reflection. Because the measurements are not corrected for different reflectance, this small step of absorbance appears. The fact that there is no plasmon peak for $t = 100$ s despite some NPs still being there, as showed by SEM, reinforces the hypothesis of the oxidation.

3.2. Top-down application: silicon nanograss synthesis

Selective synthesis of silicon nanograss was attempted by using the NPs as hard masking objects in order to show the viability of the nanoseeding method for the production of nanostructures. For this, a silicon sample was patterned with the nanocomposite, and oxygen treated. The treated silicon sample looked clean to the naked eye. The sample was then anisotropically etched using RIE rendering the patterns visible to the naked eye as shown in figure 5(a). Most of the sample looked black where the nanocomposite was placed, and shiny in the areas where no nanocomposite was located. A closer view with the SEM reveals the reason for this structural colouring effect. Areas with no NPs present a mostly even surface (figure 5(b)), with only small defects. Areas populated by the NPs are covered with silicon nano-grass (figure 5(c)), which confers the black colour to the sample. The silicon tips are about 500 nm tall, although there is some polydispersity. Some truncated cones can be clearly seen, which means that they have been masked by a NP during the etching of the silicon. The tips have been scratched on a grid and further examined on the TEM (figure 5(d)). The TEM inspection reveals tips of different sizes. The larger tips quite often present a truncated cone shape and NPs on their tip, as can be seen in figure 5(d). These NPs look dark under the TEM, which means that they have a heavy atom com-position, such as silver. The larger NPs are 40–50 nm in
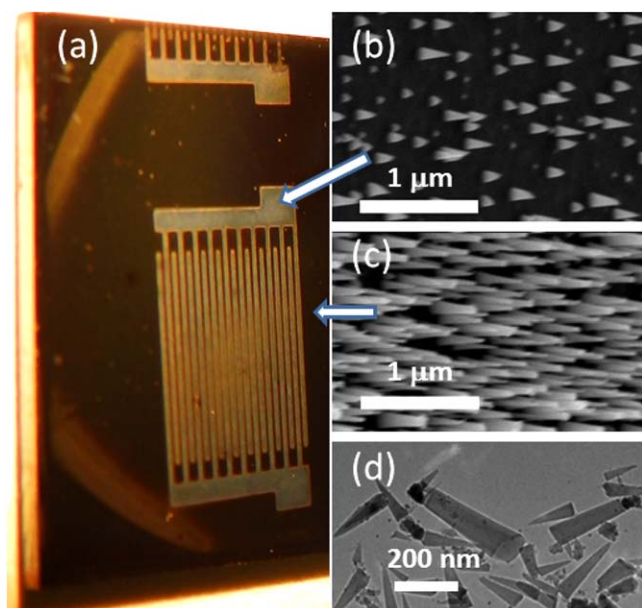
Figure 5. (a) Image of the sample treated by RIE for nanograss formation, (b) SEM of a cleared area (without NPs), (c) SEM of an area with NPs, (d) TEM of the scrapped nanowires, where some silicon structures are capped by silver NPs.
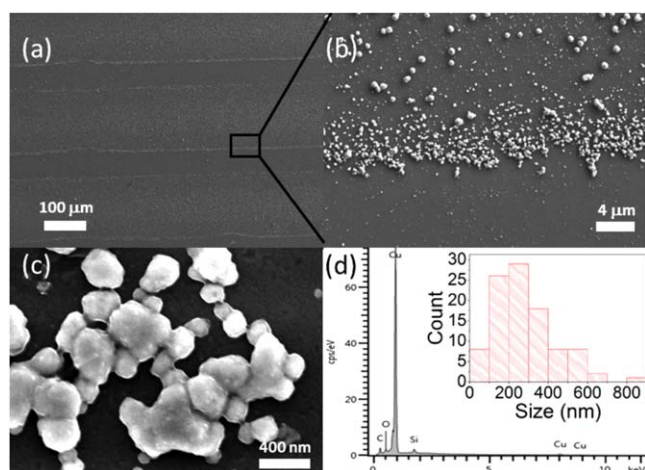

Figure 6. Selectively pattered area with copper clusters after electroless plating. The areas where the NPs were placed present copper deposition. Energy dispersive x-ray spectroscopy of a large copper particle.

diameter, which again agrees with the electron microscopy images of figures 2(b) and 3(b). The smaller tips are sharp and do not show NPs at their top. This could be explained by their origin from the masking by smaller NPs, which produce a smaller footprint. Because the RIE process is not completely anisotropic (note the conical profiles), the etching could allow undercutting below the small NPs and their subsequent release followed by the sharpening of the silicon tip.

3.3. Bottom-up application: copper nanoparticle synthesis

The nanoseeding method presented here can be used for bottom-up applications whereby the metallic NPs serve as

seeds for a variety of nanostructure growths. Figure 6 shows a silicon substrate processed as the sample of figure 3(b), which has been immersed for 10 min in a copper sulphate-based electroless plating solution [44]. Larger copper clusters selectively grow on the areas where the nanocomposite was placed.

The strong reducing character of this solution [45], which has a very high pH of the order of 12, favours the local reduction and creation of metallic sites that catalyse the later growth. Figures 6(b) and (c) show the resulting copper particles. The shape of the particles reveals that the growth is favoured in the vertical direction, producing copper clusters with a grain size of 280 ± 150 nm (insert figure 6(d)). The EDX spectrum of a measurement done on top of one of these clusters predominantly shows emission peaks of copper. The quantitative analysis reveals that 70% of the atomic percentage corresponds to copper, while the rest comes from oxygen, silicon and carbon from the background. This is expected because the collections area is approximately a square micrometre. No sulphur has been found, which means that there is no redeposited copper sulphate. It can be seen in figures 6(a)–(b) that the patterning is very selective. Figure 6(b) shows some small particles that have grown outside the desired area. This could point to some minor redeposition, since this plating formulation only allows copper growth in the presence of metallic seeds [32, 46]. This minor redeposition could be due to a distribution of the silver NPs all along the thickness of the thin film, including both interphases. This kind of distribution has been previously observed for similar systems where NPs are gown *in situ* in a thin film [47].

As future work, this method is being used to selectively create surfaces with large specific surface areas for silicon electrochemical sensors. The enhanced areas provide several advantages, and there is a demand for controllable fabrication processes [48]. Such an application does not demand high purity for the metallic NPs nor high resolution or monodispersity. However, it benefits from the availability of silicon technology for chip production as well as the accuracy of the plasma-based microfabrication techniques. Although the intended application is not sensitive to oxidation processes, for some applications it could be desirable to have pure metal. This issue could be approached by using a common technique to remove oxide from metallic surfaces prior to molecular growth, which consists of reducing the surface with a hydrogen plasma treatment. Another possibility to reduce the oxidation of the NPs would be to use gold rather than silver. Novolac has proved to be another good host for *in situ* synthesis of Au NPs [21], and gold has the advantage of being much more resistant to oxidation than silver.

4. Conclusions

In this work we have developed a general method for the selective growth of nanostructures. This method relies on the production of Ag NPs in selected areas by photolithography. As a result of the polymeric matrix, the NPs are synthesised in

a range of different sizes, where the larger NPs are about 50 nm. The fine tuning of a plasma process has allowed the predominant removal of the polymer, and exposition of the NPs. Although the evolution of the localised surface plasmon resonance of the NPs reveals their oxidation, the NPs are still useful as seeds for subsequent synthesis processes. Both top-down and bottom-up processes have been demonstrated. A fluoride-based RIE has been used to produce silicon nanotips by using the NPs as hard mask. The hard masking effect is revealed by the presence of truncated cones. The NPs have also demonstrated useful as seeds for the selective growth of copper clusters. The flexibility of the method allows its use in a multitude of applications, and it is currently being used for sensor array fabrication.

Acknowledgments

ORCID iDs

J Marques-Hueso ⓘ https://orcid.org/0000-0002-1807-3369
Xiangfu Wang ⓘ https://orcid.org/0000-0003-2365-3357

References

[1] Gates B D, Xu Q, Love J C, Wolfe D B and Whitesides G M 2004 Unconventional Nanofabrication *Annu. Rev. Mater. Res.* **34** 339–72

[2] Schlücker S 2014 Surface-enhanced raman spectroscopy: concepts and chemical applications *Angew. Chem. Int. Ed.* **53** 4756–95

[3] Judith L, Sergey M N and Luis M L-M 2015 Sensing using plasmonic nanostructures and nanoparticles *Nanotechnology* **26** 322001

[4] Emmanuel F and Samuel G 2008 Surface enhanced fluorescence *J. Phys. D: Appl. Phys.* **41** 013001

[5] Santos A, Deen M J and Marsal L F 2015 Low-cost fabrication technologies for nanostructures: state-of-the-art and potential *Nanotechnology* **26** 042001

[6] Roberts N A, Fowlkes J D, Mahady K, Afkhami S, Kondic L and Rack P D 2013 Directed assembly of one- and two-dimensional nanoparticle arrays from pulsed laser induced dewetting of square waveforms *ACS Appl. Mater. Interfaces* **5** 4450–6

[7] Jacopo F, Gabriele S, Sabina S, Michele P and Luca B 2015 Fabrication of periodic arrays of metallic nanoparticles by block copolymer templates on HfO$_2$ substrates *Nanotechnology* **26** 215301

[8] Tatiana N S, Lyudmila M K, Alexander S K, Oksana V S and Joachim S 2009 The fabrication of periodic polymer/silver nanoparticle structures: *in situ* reduction of silver nanoparticles from precursor spatially distributed in polymer using holographic exposure *Nanotechnology* **20** 405301

[9] Robert A H, Eredzhep M and Svetlana N 2017 When lithography meets self-assembly: a review of recent advances in the directed assembly of complex metal nanostructures on planar and textured surfaces *Nanotechnology* **28** 282002

[10] Yang S-M, Jang S G, Choi D-G, Kim S and Yu H K 2006 Nanomachining by colloidal lithography *Small* **2** 458–75

[11] Awan K M, Sanatinia R and Anand S 2014 Nanostructuring of GaAs with tailored topologies using colloidal lithography and dry etching *J. Vac. Sci. Technol.* B **32** 021801

[12] Sun H, Yu M, Wang G, Sun X and Lian J 2012 Temperature-dependent morphology evolution and surface plasmon absorption of ultrathin gold island films *J. Phys. Chem.* C **116** 9000–8

[13] Ramesh G V, Porel S and Radhakrishnan T P 2009 Polymer thin films embedded with *in situ* grown metal nanoparticles *Chem. Soc. Rev.* **38** 2646–56

[14] Abargues R, Abderrafi K, Pedrueza E, Gradess R, Marques-Hueso J, Valdes J L and Martinez-Pastor J 2009 Optical properties of different polymer thin films containing *in situ* synthesized Ag and Au nanoparticles *New J. Chem.* **33** 1720–5

[15] Pan D *et al* 2014 Controlled synthesis of phase-pure InAs nanowires on Si(111) by diminishing the diameter to 10 nm *Nano Lett.* **14** 1214–20

[16] Leroy F, Borowik Ł, Cheynis F, Almadori Y, Curiotto S, Trautmann M, Barbé J C and Müller P 2016 How to control solid state dewetting: a short review *Surf. Sci. Rep.* **71** 391–409

[17] Marques-Hueso J, Abargues R, Canet-Ferrer J, Valdes J L and Martinez-Pastor J 2010 Resist-based silver nanocomposites synthesized by lithographic methods *Microelectron. Eng.* **87** 1147–9

[18] Marques-Hueso J, Abargues R, Canet-Ferrer J, Agouram S, Valdés J L and Martínez-Pastor J P 2010 Au-PVA nanocomposite negative resist for one-step three-dimensional e-beam lithography *Langmuir* **26** 2825–30

[19] Abargues R, Marques-Hueso J, Canet-Ferrer J, Pedrueza E, Valdés J L, Jiménez E and Martínez-Pastor J P 2008 High-resolution electron-beam patternable nanocomposite containing metal nanoparticles for plasmonics *Nanotechnology* **19** 355308

[20] Marques-Hueso J, Abargues R, Valdes J L and Martinez-Pastor J P 2010 Ag and Au/DNQ-novolac nanocomposites patternable by ultraviolet lithography: a fast route to plasmonic sensor microfabrication *J. Mater. Chem.* **20** 7436–43

[21] Marques-Hueso J, Abargues R, Richards B S, Valdes J L and Martinez-Pastor J P 2012 Plasmon damping in Ag-nanoparticles/polymer composite for optical detection of amines and thiols vapors *SPIE Photonics Eur.* (*Nanophotonics IV* 8424) (*Brussels, Belgium, 30 April 2012*) 842410

[22] Pudlauskaitė J, Jankauskaitė V, Lazauskas A, Prosyčevas I and Narmontas P 2013 Ag/DNQ-novolac-based nanocomposite films for controllable UV lithography morphological patterning *Colloid Polym. Sci.* **291** 1787–93

[23] Yonatan C, Alexander K, Dor A, Arkady G, Shimon C and Dan R 2016 Reduction of nanowire diameter beyond lithography limits by controlled catalyst dewetting *J. Phys. D: Appl. Phys.* **49** 165309

[24] Wu B and Kumar A 2014 Extreme ultraviolet lithography and three dimensional integrated circuit—a review *Appl. Phys. Rev.* **1** 011104

[25] Takagi D, Homma Y, Hibino H, Suzuki S and Kobayashi Y 2006 Single-walled carbon nanotube growth from highly activated metal nanoparticles *Nano Lett.* **6** 2642–5

[26] Wagner R S and Ellis W C 1964 Vapor-liquid-solid mechanism of single crystal growth *Appl. Phys. Lett.* **4** 89–90

[27] Schmidt V, Wittemann J V, Senz S and Gösele U 2009 Silicon nanowires: a review on aspects of their growth and their electrical properties *Adv. Mater.* **21** 2681–702

[28] Tsivion D, Schvartzman M, Popovitz-Biro R, von Huth P and Joselevich E 2011 Guided growth of millimeter-long horizontal nanowires with controlled orientations *Science* **333** 1003–7

[29] Kayes B M, Filler M A, Putnam M C, Kelzenberg M D, Lewis N S and Atwater H A 2007 Growth of vertically aligned Si wire arrays over large areas (>1 cm^2) with Au and Cu catalysts *Appl. Phys. Lett.* **91** 103110

[30] Zopes D, Von Hagen R, Muller R, Fiz R and Mathur S 2010 Ink-jetable patterning of metal-catalysts for regioselective growth of nanowires *Nanoscale* **2** 2091–5

[31] Seth A F and Xiuling L 2010 Metal-catalyzed semiconductor nanowires: a review on the control of growth directions *Semicond. Sci. Technol.* **25** 024005

[32] Marques-Hueso J, Jones T D A, Watson D E, Ryspayeva A, Nekouie Esfahani M, Shuttleworth M P, Harris R A, Kay R W and Desmulliez M P Y 2018 A rapid photopatterning method for selective plating of 2D and 3D microcircuitry on polyetherimide *Adv. Funct. Mater.* **28** 1704451

[33] Denver P L, Huu Khuong Duy N, Chris M B, Saulius J and Elena P I 2017 Influence of nanoscale topology on bactericidal efficiency of black silicon surfaces *Nanotechnology* **28** 245301

[34] Pecora E F, Lawrence N, Gregg P, Trevino J, Artoni P, Irrera A, Priolo F and Negro L D 2012 Nanopatterning of silicon nanowires for enhancing visible photoluminescence *Nanoscale* **4** 2863–6

[35] Wang C, Luo F, Lu H, Liu B, Chu G, Quan B, Li J, Gu C, Li H and Chen L 2017 Side-by-side observation of the interfacial improvement of vertical graphene-coated silicon nanocone anodes for lithium-ion batteries by patterning technology *Nanoscale* **9** 17241–7

[36] Liu X, Coxon P R, Peters M, Hoex B, Cole J M and Fray D J 2014 Black silicon: fabrication methods, properties and solar energy applications *Energy Environ. Sci.* **7** 3223–63

[37] Otto M *et al* 2015 Black silicon photovoltaics *Adv. Opt. Mater.* **3** 147–64

[38] Nadine G, Nicole W, Bodo F, Alexander T, Andreas B, Peter W, Marco J, Reinhard K-R and Hartmut S L 2015 Influence of the doping level on the porosity of silicon nanowires prepared by metal-assisted chemical etching *Nanotechnology* **26** 245301

[39] Jansen H, Boer M D, Legtenberg R and Elwenspoek M 1995 The black silicon method: a universal method for determining the parameter setting of a fluorine-based reactive ion etcher in deep silicon trench etching with profile control *J. Micromech. Microeng.* **5** 115

[40] Jansen H, De Boer M, Burger J, Legtenberg R and Elwenspoek M 1995 The black silicon method: II. The effect of mask material and loading on the reactive ion etching of deep silicon trenches *Microelectron. Eng.* **27** 475–80

[41] Williams K R, Gupta K and Wasilik M 2003 Etch rates for micromachining processing: II *Microelectromech. Syst., J.* **12** 761–78

[42] Carlberg B, Ye L-L and Liu J 2011 Surface-confined synthesis of silver nanoparticle composite coating on electrospun polyimide nanofibers *Small* **7** 3057–66

[43] Rooij A D 1989 The oxidation of silver by atomic oxygen *ESA J.* **3** 363–82

[44] Hidber P C, Helbig W, Kim E and Whitesides G M 1996 Microcontact printing of palladium colloids: micron-scale patterning by electroless deposition of copper *Langmuir* **12** 1375–80

[45] Niino H and Yabe A 1992 Positively charged surface potential of polymer films after excimer laser ablation: application to selective-area electroless plating on the ablated films *Appl. Phys. Lett.* **60** 2697–9

[46] Jones T D A, Ryspayeva A, Esfahani M N, Shuttleworth M P, Harris R A, Kay R W, Desmulliez M P Y and Marques-Hueso J 2018 Direct metallisation of polyetherimide substrates by activation with different metals *Appl. Surf. Sci.* submitted

[47] Pedrueza E, Valdés J L, Chirvony V, Abargues R, Hernández-Saz J, Herrera M, Molina S I and Martínez-Pastor J P 2011 Novel method of preparation of gold-nanoparticle-doped TiO$_2$ and SiO$_2$ plasmonic thin films: optical characterization and comparison with Maxwell–Garnett modeling *Adv. Funct. Mater.* **21** 3502–7

[48] Kim D-J, Ha D, Zhou Q, Thokchom A K, Lim J W, Lee J, Park J G and Kim T 2017 A cracking-assisted micro-/nanofluidic fabrication platform for silver nanobelt arrays and nanosensors *Nanoscale* **9** 9622–30